



Method for honey bee MALDI imaging

Deliverable D9.14

16 May 2022

Author(s): Karim Arafah¹⁾, Dalel Askri¹⁾, Sébastien Voisin¹⁾ & Philippe Bulet²⁾

¹⁾Plateforme BioPark d'Archamps, Archamps, France

²⁾CR, University Grenoble Alpes, IAB Inserm 1209, CNRS UMR5309, Grenoble, France

PoshBee

**Pan-european assessment, monitoring, and mitigation
of stressors on the health of bees**



Prepared under contract from the European Commission

Grant agreement No. 773921

EU Horizon 2020 Research and Innovation action

Project acronym: **PoshBee**
 Project full title: **Pan-european assessment, monitoring, and mitigation of stressors on the health of bee**
 Start of the project: June 2018
 Duration: 60 months
 Project coordinator: Professor Mark Brown
 Royal Holloway and Bedford New College www.poshbee.eu

Deliverable title: Method for honey bee MALDI imaging
 Deliverable n°: D9.14
 Nature of the deliverable: Other
 Dissemination level: Public

WP responsible: WP9
 Lead beneficiary: CNRS

Citation: Arafah, K., Askri, D., Voisin, S. & Bulet, P. (2022). *Method for honey bee MALDI imaging*. Deliverable D9.14 EU Horizon 2020 PoshBee Project, Grant agreement No. 773921.

Due date of deliverable: Month n°48
 Actual submission date: Month n°48

Deliverable status:

Version	Status	Date	Author(s)
1.0	Final	16 May 2022	Karim Arafah ¹⁾ , Dalel Askri ¹⁾ , Sébastien Voisin ¹⁾ & Philippe Bulet ²⁾ ¹⁾ Plateforme BioPark d'Archamps, Archamps, France ²⁾ CR, University Grenoble Alpes, IAB Inserm U1209, CNRS UMR 5309, Grenoble, France

The content of this deliverable does not necessarily reflect the official opinions of the European Commission or other institutions of the European Union.

Table of contents

Preface	4
1. Overview of the MALDI imaging workflow	4
2. Detailed MALDI imaging workflow.....	5
2.1 Sample preparation: honey bee inclusion, positioning and cryosectioning.....	5
2.2 Preparation of the samples for MALDI analysis (figure 4)	7
2.3 Data acquisition and processing	7
3. MALDI IMS workflow experimented to evaluate the impact of <i>Nosema</i> on <i>Apis mellifera</i>	9
4. Conclusions on MALDI imaging tested on Nosemosis	12
5. Perspectives	12
6. References.....	12

Preface

MALDI Imaging Mass Spectrometry (IMS) is widely used in life sciences, biomedical and pharmaceutical research as an imaging technique in the biological investigation of molecular responses to xenobiotic and endogenous processes across various biological matrices (Schulz *et al.*, 2019; Swales *et al.*, 2018). Advancements in instrumentation for improved resolution and sensitivity, sample preparation workflows including innovative chemical strategies for on-tissue chemical derivatisation or to generate novel matrices, and data management and processing, offer the ability to precisely quantify tissue molecular abundances at a high-resolution level (Chumbley *et al.*, 2016; Källback *et al.*, 2016; Porta *et al.*, 2015; Rzagalinski *et al.*, 2017; Zhou *et al.*, 2020). MALDI IMS technology is now used to analyse biological samples belonging to both plant (Boughton *et al.*, 2018; Dong *et al.*, 2016; Qin *et al.*, 2018; Susniak *et al.*, 2020) and animal kingdoms, including human specimens (Schulz *et al.*, 2019; Harris *et al.*, 2020; Seeley *et al.*, 2011). Given the increasing use of MALDI IMS on vertebrate models, this approach has also been investigated in different invertebrate models and for the first time in insects to map neuropeptides within the neuronal tissues of the cricket *Acheta domestica* (Verhaert *et al.*, 2007). Subsequently, MALDI IMS was applied to bee models to follow the distribution of queen-signal compounds (Nunes *et al.*, 2015), to analyse the neuropeptide distribution in the Africanised honey bee (*Apis mellifera*) brain (Pratavieira *et al.*, 2014; 2018) or to follow the degradation and toxicity of pesticides (Catae *et al.*, 2014; 2018a; 2018b) and to identify the most abundant metabolites (Pratavieira *et al.*, 2020). Very recently (May 2022), Zhang and colleagues published a study on the stereoselective toxicity mechanism of neonicotinoid dinotefuran in honey bees (Zhang *et al.*, 2022).

In this report, the key steps of the method for honey bee MALDI imaging are presented in the form of an experimental workflow applied to an experimental infection with the biotic stressor responsible for nosemosis, an important honey bee disease. Specifically, this workflow was designed as a reproducible protocol to map peptides and proteins up to 15kDa directly on whole body tissue sections of *Apis mellifera*. This workflow was applied for the first time, as a case study, on an experimental model of infection with spores of the causative agent of nosemosis, the microsporidian *Nosema*, in order to image its molecular impact at a spatio-temporal level on different organs of the bee. The designed method for honey bee MALDI imaging proposed in this deliverable can be applied to other pollinators following minor adjustments.

1. Overview of the MALDI imaging workflow

In summary, MALDI IMS is based on a scan examination of the protein distribution in the body of a bee following four major steps (see **figure 1**):

1. Collection of bees that have been experimentally stressed or not (honey bee sample).
2. Perfusion and inclusion of the body in specific chemicals and embedding at a defined orientation to visualise tissues of interest in cryosections (histological blocks and cryosections).
3. Sample preparation (including desalting + delipidation) and scan examination by MALDI mass spectrometer dedicated to imaging (scan examination-IMS).
4. Data processing to provide molecular images on the localisation of peptides and proteins within tissues in control *versus* a stress condition (body scan merged with body anatomy and image analysis).

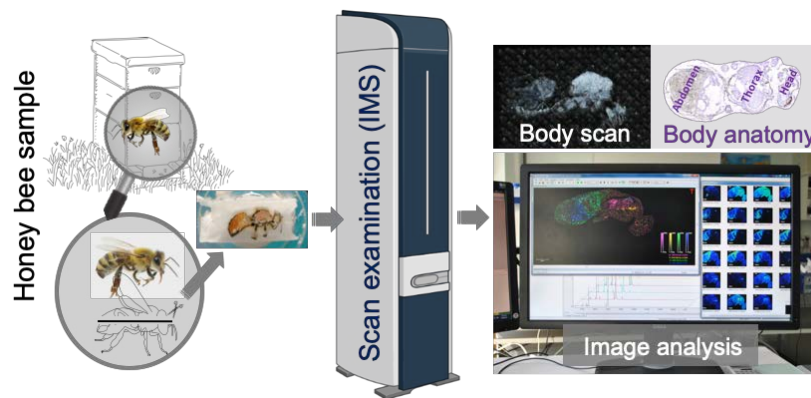


Figure 1: Graphical abstract summarising the experimental workflow including from bee collection to image analysis.

2. Detailed MALDI imaging workflow

2.1 Sample preparation: honey bee perfusion and inclusion, positioning and cryosectioning

To obtain histological blocks for MALDI IMS, honey bees were first anaesthetised using carbon dioxide and individually embedded into a 2% (w:v) solution of low viscosity 90kDa carboxymethyl cellulose (CMC, Sigma Aldrich, France) polymer prepared in ultrapure water. Additionally, the embedded bees were instantaneously vented for 20 minutes under 600 mbar vacuum using a home-made device apparatus to ensure optimal perfusion and inclusion of bee bodies. The remaining air from the bees' respiratory system and from the vicinity of their cuticles was thereby substituted with the low viscosity CMC. The prepared bodies were then transferred into a filled tube with a chilled solution of the 250kDa CMC polymer (see **comment n°1**). Once prepared, the samples were stored at -80°C for 24 hours before being sliced using a cryomicrotome. Cryosections ($15\mu\text{m}$ thickness) of the whole bee body were transferred onto ITO-conductive glass slides (Bruker GmbH). Before being sliced, the CMC-embedded body blocks were transferred from -80°C inside a cryomicrotome (Leica CM1950, Germany) maintained at -20°C and left to reach this appropriate cutting temperature for 15 minutes.

Serial fresh frozen cryosections ($15\mu\text{m}$ thickness) were collected either onto classical histological slides (Dominique Dutscher, France), stained for 20 seconds with haematoxylin for histological mapping of the organs, or transferred onto conductive Indium Tin Oxide (ITO)-coated glass slides (Bruker GmbH, Germany) for MALDI IMS. The fresh frozen cryosections were digitised using the Nikon CoolScan 9000 (Nikon, Japan) to "teach" the MALDI IMS automated process and a high-resolution desktop microscope Mirax (Zeiss, Germany) was used for observations of histological features (**figure 2**).

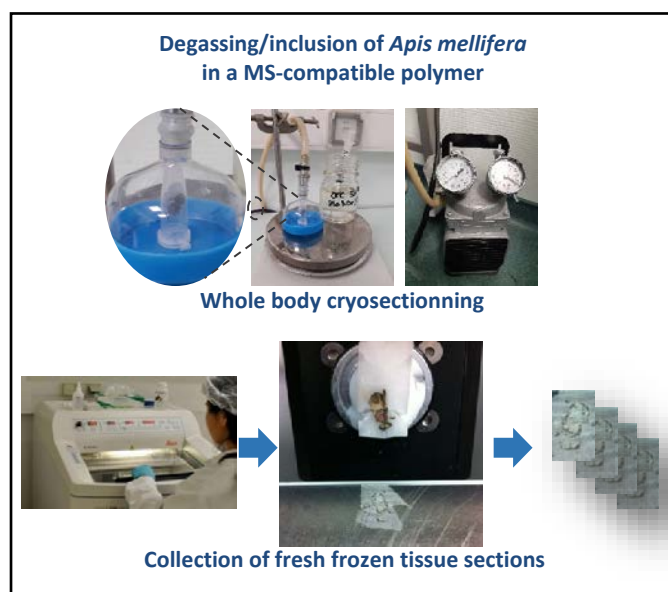


Figure 2: First step of the workflow, including sample preparation: honey bee degassing and inclusion, degassing, positioning for embedding, and whole body cryosectioning.

Comment n°1: To obtain an exhaustive image of the impact of a stressor on *A. mellifera*, the CMC embedded body blocks were cryosliced according to sagittal and frontal planes to image as many organs as possible that may be direct or indirect targets of the stressor(s) (e.g., infectious, pesticide). We initiated MALDI images of *A. mellifera* in a sagittal plane followed by sections in a frontal plane.

Before proceeding with MALDI IMS, to avoid excess of salts and lipids, the ITO-conductive glass slides with the bee body slices were washed in three successive baths of pure ethanol (immersion only followed by total drying of slice between each rinsing), and a one-second immersion in pure chloroform (see **comment n°2** and **figure 3**).

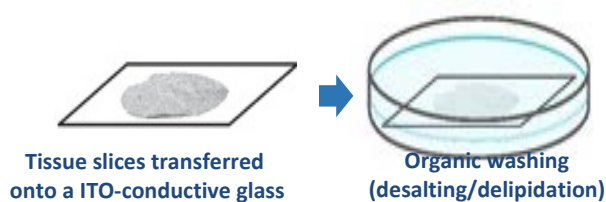


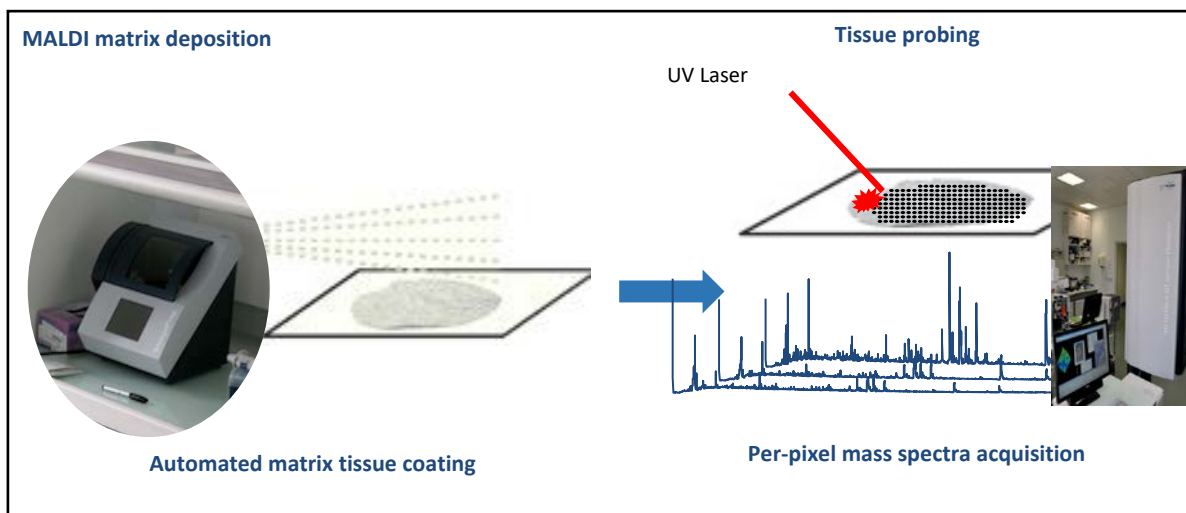
Figure 3: Desalting and delipidation of the bee slices using organic washing with pure ethanol followed by pure chloroform.

Comment n°2: Prior to perfusion, embedding and slicing, we first tested a combination of solvents to delipidate and desalt the tissue sections, a depletion step deemed important to optimise peptide/protein detection. We tried various combinations of depletion. At the beginning of our experiments, we used only ethanol but we rapidly observed an improvement of spectra acquisition with the addition of chloroform.

2.2 Preparation of the samples for MALDI analysis (figure 4)

As a first step, a matrix coating of the cuts on ITO slides is required using an automated piezoelectric nebulizer (ImagePrep, Bruker GmbH, Germany). After evaluating several matrices, compositions and deposition programs (see **comment n°3**), the best results were obtained using tissue sections coated with a solution of 2,5 Dihydroxybenzoic acid (DHB) at 20 mg/mL in MeOH/Water (50/50; v/v) acidified with 0.2 % TFA final concentration. This matrix solution was sprayed in two runs with the ImagePrep nebulizer (Bruker GmbH, Germany) following recommendations provided by the manufacturer (DHB_standard_1).

Figure 4: Preparation of samples for MALDI analysis, matrix deposition and tissue probing for



spectral acquisition using a laser for desorption of peptides of proteins from the bee tissues.

Comment n°3: we evaluated the quality of recorded spectral signal from direct tissue imaging using Sinapinic acid (SA), α -Cyano-4-hydroxycinnamic acid (4-HCCA) and 2,5 Dihydroxybenzoic acid (DHB), the three most frequently employed matrices. To assess tissue complexity, we looked at the ionic signal recorded from body segments (head, thorax, abdomen) through targeted tissue imaging of region of interest (ROI) versus whole body sections.

2.3 Data acquisition and processing

MALDI IMS spectra (mass range 1,000-18,000 m/z) were acquired in a positive ion linear mode using an AutoFlex™ III SmartBeam MALDI mass spectrometer equipped with a 200 Hz 355-nm frequency-tripled Nd:YAG laser (Bruker Daltonics, Germany) and laser probing of the whole bee body tissue surface used MALDI MS (AutoFlex III, lateral resolution 60 μ m, Bruker GmbH) according to the analytical conditions and MALDI datasets processing as summarised in **table I** and **figure 5**.

The instrument was calibrated using a mixture of two sets of peptides (APISCAL) and proteins (ProtMix) covering the dynamic range of interest. The composition of the homemade APISCAL is as follows: synthetic pure Apidaecin and Abaecin, two antimicrobial peptides from *Apis mellifera* (average m/z of 2109 and 3879, respectively), synthetic pure melittin, the major venom component, (average m/z of 2847); and ETD, a recombinant peptide, (average m/z of 4839). ProtMix (Protein Calibration Standard I, Bruker Daltonics) is a manufacturer-available mixture of four peptides and

proteins (Insulin, Ubiquitin, Cytochrome C and Myoglobin at average m/z of 5734, 8565, 12,360, and 16,952, respectively).

Table I: Analytical parameters selected to acquire molecular images by MALDI imaging and for their statistical analysis

Analytical parameters used to perform tissular MALDI MFPs and imaging		
	MALDI Mass Fingerprinting	MALDI Imaging
MALDI-TOF/TOF Equipment	AutoFlex III	
Digitizer	Acqiris DP240 version 1.16	
UV Laser type	Smartbeam™ laser (v2_0_11_0)	
Piloting software	FlexControl 3.4 software (build 135.12)	
Polarity	Positive	
Laser frequency(Hz)	200	200
Laser shots sum per position	1,000	1,000
Laser power (%)	55	80
Laser focus mode	MBT	Ultra
Global attenuation offset (%)	40	60
Accelerating voltage (kV)	1.30	1.50
Lens voltage (kV)	9.25	9.02
Pulsed ion extraction delay (ns)	120	140
Gating (Da)	600	1,000
Detector Gain	28X (1906V)	51X (1999V)
m/z range of analysis	600-18,000	1,000-20,000
Spatial resolution (μm)	Not concerned	60
Spectra visualization and processing	FlexAnalysis 3.4 (Bruker Daltonik, Germany)	FlexImaging 4.1 (build 116, FC_Clinprot method) and SciLS Lab 2D software (version 3.02.7817), SCiLS Lab/Bruker Daltonik, Germany
Spectra annotation	mMass v5.5	
Baseline correction / smoothing algorithm	TopHat / Savitzky-Golay (5.0 m/z window size, 2 cycles)	TopHat (width 200)
Peak annotation signal-to-noise ratio / Peak height	3.0 / 75	manual peak-picking
Cut-off for peak selection (kDa)	1.0	1.0

Analytical parameters used to perform tissular MALDI MFPs and imaging		
	MALDI Mass Fingerprinting	MALDI Imaging
MALDI-TOF/TOF Equipment	AutoFlex III	
Digitizer	Acqiris DP240 version 1.16	
UV Laser type	Smartbeam™ laser (v2_0_11_0)	
Piloting software	FlexControl 3.4 software (build 135.12)	
Polarity	Positive	
Laser frequency(Hz)	200	200
Laser shots sum per position	1,000	1,000
Laser power (%)	55	80
Laser focus mode	MBT	Ultra
Global attenuation offset (%)	40	60
Accelerating voltage (kV)	1.30	1.50
Lens voltage (kV)	9.25	9.02
Pulsed ion extraction delay (ns)	120	140
Gating (Da)	600	1,000
Detector Gain	28X (1906V)	51X (1999V)
m/z range of analysis	600-18,000	1,000-20,000
Spatial resolution (μm)	Not concerned	60
Spectra visualization and processing	FlexAnalysis 3.4 (Bruker Daltonik, Germany)	FlexImaging 4.1 (build 116, FC_Clinprot method) and SciLS Lab 2D software (version 3.02.7817), SCiLS Lab/Bruker Daltonik, Germany
Spectra annotation	mMass v5.5	
Baseline correction / smoothing algorithm	TopHat / Savitzky-Golay (5.0 m/z window size, 2 cycles)	TopHat (width 200)
Peak annotation signal-to-noise ratio / Peak height	3.0 / 75	manual peak-picking
Cut-off for peak selection (kDa)	1.0	1.0

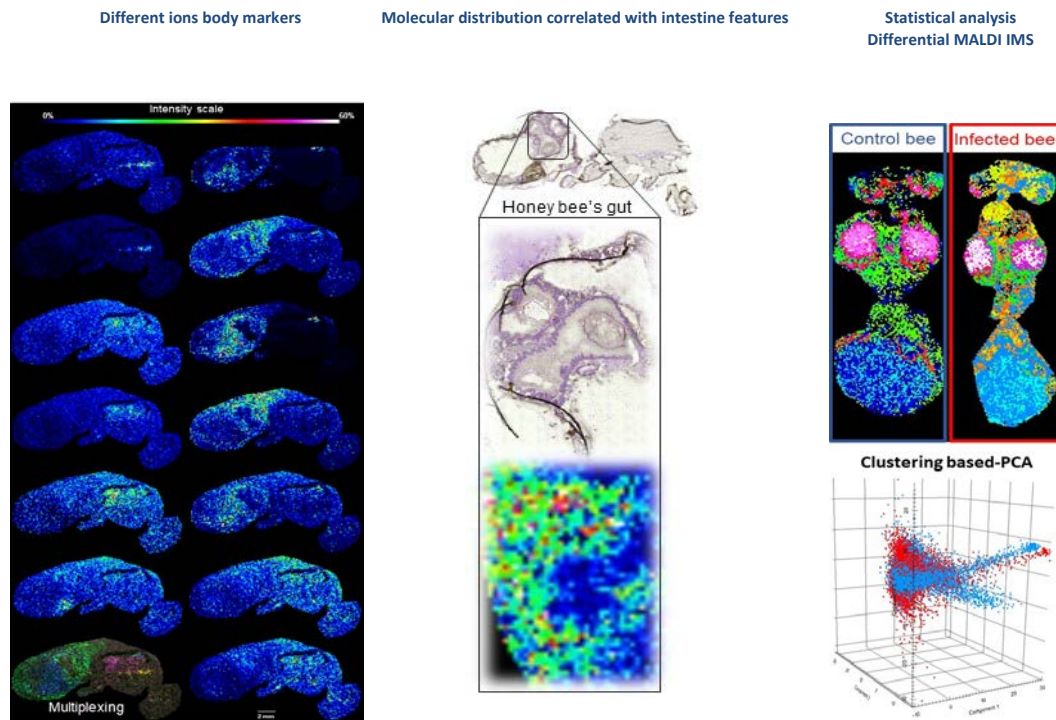


Figure 5: Per-pixel ion density mapping in whole bee body sections. Different dedicated software programmes (list provided in table I) were used to process the spectral acquisitions and to generate images and statistical issues such as clustering-based Principal Component Analysis (PCA). This figure is derived from Houdelet et al., 2022)

3. MALDI IMS workflow used to evaluate the impact of *Nosema* on *Apis mellifera*

We successfully applied this MALDI IMS protocol to follow the molecular impact of an experimental infection (16 days post infection) with spores of the microsporidian *Nosema ceranae* on newly emerged *A. mellifera*. Firstly, we optimised the workflows on non-experimentally infected bees (N-). **Figure 6** below reports a set of data to evidence organ visualisation through a selected short list (the entire list is available in Houdelet *et al.*, 2022) of recorded molecular ions (peptides and proteins). This organ visualisation establishes an initial bee histo-molecular atlas, obtained using frontal plane sections. We initiated MALDI IMS on sagittal plane sections. However, with such a sectioning plane poor tissue resolution was obtained for the anatomical sections of the gut making it difficult to visualise the brain, thoracic ganglia and especially the ventral ganglia.

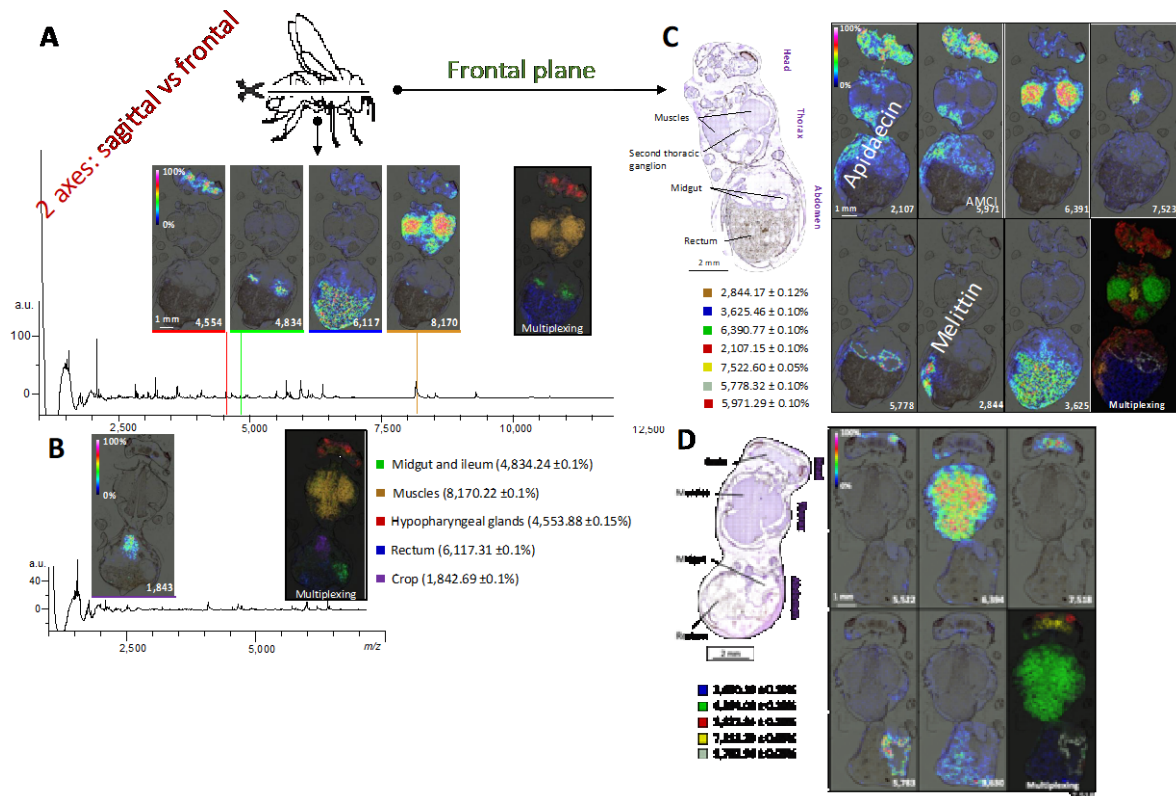


Figure 6: Selected images to illustrate the data from MALDI imaging on *Apis mellifera*. Molecular mass spectra and images of markers identified by MFPs extracted from MALDI IMS analyses of frontal whole-body sections of *Apis mellifera*. The potential markers of the hypopharyngeal glands (red), rectum (blue), muscles (orange), the midgut and ileum (green) were found in the general mass spectra on a first bee section (A) and the crop (purple) on a second bee section (B). Molecular images of markers identifying bee tissues/organs. (C) Haematoxylin stained section of one honey bee cryosection showing the muscles, second thoracic ganglion, midgut and rectum, and MALDI images with tissue specific molecular-related ion markers. (D) Another honey bee (stained) cryosection showing the muscles, brain, midgut and rectum. The associated molecular images were observed and pictured in the specific tissues. All values on pictures are expressed in m/z. Bar scale: 1mm. Scale of intensity from 0 to 100% of the molecular-related ions.

Secondly, we translated this procedure to bees experimentally infected with *Nosema* spores (N+). The detailed methodology to prepare the infected bees, the mass spectrometry analysis and the most probing results, conclusions and perspectives of this differential molecular imaging analysis (N+ vs N-) performed *in situ* are available in the publication of Houdelet and colleagues (2022) and in her PhD thesis (available in French at <https://www.theses.fr/252930428>). As expected, a distinction in these molecular profiles between the two conditions was observed in different anatomical sections of the gut tissue, the initial target for the microsporidia. More importantly, we observed (see figure 7) differences in the molecular profiles in the (i) brain, (ii) thoracic ganglia, (iii) hypopharyngeal gland, and (iv) haemolymph. Through this proof of concept, we introduced MALDI IMS as an effective approach to monitor the impact of the microsporidian *Nosema ceranae* on different tissues of *A. mellifera*.

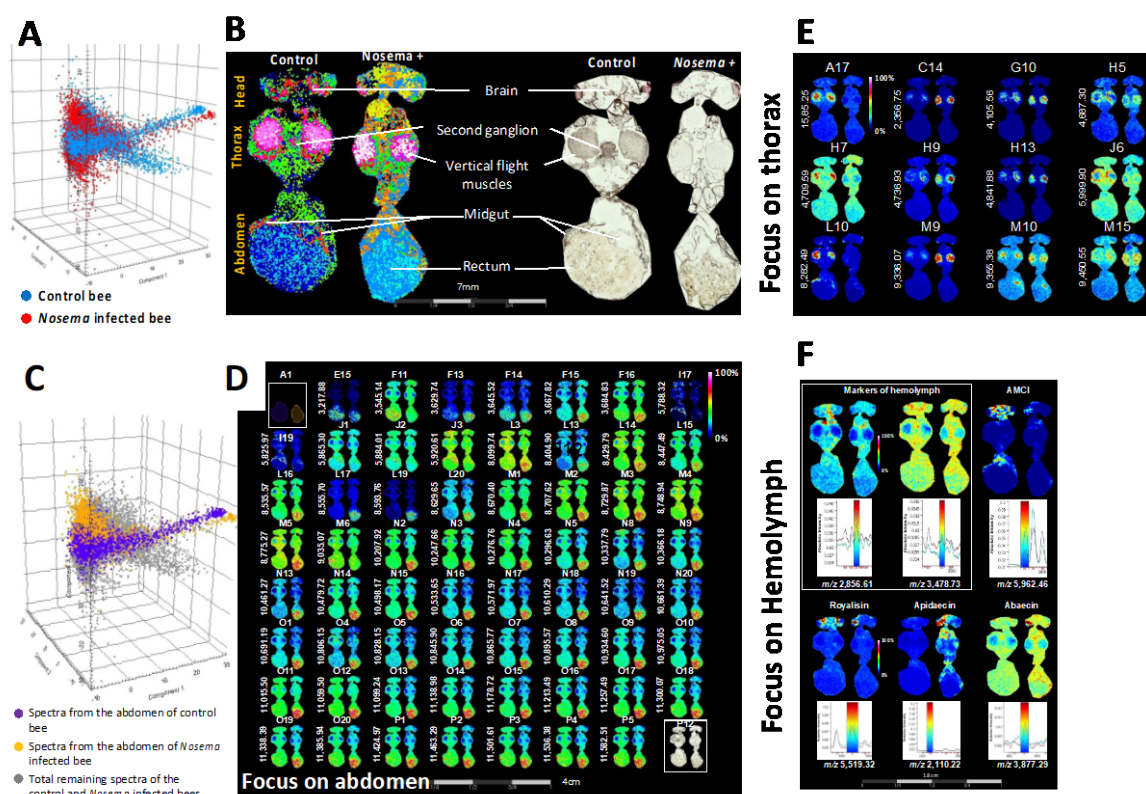


Figure 7: Differential histo-proteomics changes in *A. mellifera* following an experimental infection with spores of *Nosema ceranae*. Principal component analysis (PCA) and spatial segmentation of whole-body imaging spectra from *A. mellifera*. The spectra were submitted to unsupervised PCA (A), which discriminated the *Nosema*-infected honey bee from the control bee. The PCA-based molecular segmentation (B) evidenced specific clusters of spectra signatures through colour patterns that match with histological features (right body pictures). Discriminant PCA and differential ion patterns in the abdomen from control versus infected honey bee. The PCA analysis made with spectra from *Nosema*-infected vs control abdomens harboured different molecular patterns (C) and ions specifically expressed in either the nosemosis (right body) or in the control condition (left body) (D). The P12 coordinate corresponds to the histological view. (E) Tile view of twelve differentially expressed molecular ions in the bees' thorax following infection with *N. ceranae*. The mapped molecular-related ions (m/z) were differentially displayed between the control condition (left body) and the *Nosema*-infected bee (right body). (F) Differential abundance

intensities and mapping of characteristic markers expressed in the haemolymph, the hypopharyngeal gland and the thoracic muscles with respect to the histology and physiology of the honey bee. Two molecular-related ions correlating with the haemolymph (m/z 2856.61 and 3478.73) were found as markers (m/z 2856.61 and 3478.73). The *A. mellifera* chymotrypsin inhibitor (AMCI) was found to be most expressed in the haemolymph in the head and abdomen (m/z 5962.46) of the control experiment. The Royalisin (m/z 5519.32) was found in the head, while Apidaecin (m/z 2110.22) and Abaecin (m/z 3877.29) were found correlated with haemolymph in the head, thorax, and abdomen. The molecular-related ions are detailed in Table S4 of Houdelet and colleagues. (2022) and are identifiable through their coordinates (e.g., A17, C14, G10, H5, and P12). Intensity scale from 0% to 100% of the molecular-related ions.

4. Conclusions on MALDI imaging tested on Nosemosis

When applied to *Apis mellifera* experimentally infected with *Nosema* spores, MALDI IMS allowed us to confirm that the proteomic pattern in the gut tissue is modified compared to the one recorded from a control (non-experimentally and non-naturally infected) bee. In addition, this approach of mass spectrometry scanning showed for the same bees that (i) the haemolymph (the read-out of bee immunity) also carries information on the impact of nosemosis on bee immunity, and (ii) unexpectedly that the bee thoracic muscles are also impacted.

5. Perspectives

A new experiment on *A. mellifera* from partner 12-INRAe within PoshBee will be conducted in May-June 2022. The discussions between 10-BIOP, 11-CNRS and 12-INRA were initiated during AGM4 and the experimental plane definitively setup early April 2022. Briefly, we will have four experimental conditions (control, sulfoxaflo, virus and sulfoxaflo + virus). The bees will be exposed to sulfoxaflo for 24h and infected. They will then be used for haemolymph collection and imaging. Four bees per condition will be embedded (16 bees in total) at the 12-INRA site by Karim Arafah (10-BIOP) and two images per bee per condition (8 images in total) will be recorded and analysed at the 10-BIOP site. In parallel to the IMS analyses, the haemolymph will be collected from a series of bees for MALDI BeeTyping® analyses in order to run both techniques in parallel.

6. References

- Boughton, B. A. & Thinakaran, D. Mass Spectrometry Imaging (MSI) for Plant Metabolomics. in Plant Metabolomics (ed. António, C.) vol. 1778 241-252 (Springer New York, 2018) doi: 10.1007/978-1-4939-7819-9_17.
- Catae, A.F., Roat, T.C., Oliveira, R.A.D., Nocelli, R.C.F. & Malaspina, O. Cytotoxic effects of thiamethoxam in the midgut and malpighian tubules of Africanized *Apis mellifera* (Hymenoptera: Apidae). *Microsc. Res. Tech.* **77**, 274-281 (2014) doi: 10.1002/jemt.22339.
- Catae, A.F., da Silva Menegasso, A.R., Pratavieira, M., Palma, M.S., Malaspina, O., Roat, T.C. MALDI-imaging analyses of honeybee brains exposed to a neonicotinoid insecticide: MALDI-imaging of honeybee brains. *Pest Manag. Sci.* **75**, 607-615 (2018) doi: 10.1002/ps.5226.

- Catae, A.F., Roat, T.C., Pratavieira, M., da Silva Menegasso, A.R., Palma, M.S., Malaspina, O. Exposure to a sublethal concentration of imidacloprid and the side effects on target and nontarget organs of *Apis mellifera* (Hymenoptera, Apidae). *Ecotoxicology* **27**, 109-121 (2018) doi: 10.1007/s10646-017-1874-4.
- Chumbley, C. W. et al. Absolute Quantitative MALDI Imaging Mass Spectrometry: A Case of Rifampicin in Liver Tissues. *Anal. Chem.* **88**, 2392-2398 (2016) doi: 10.1021/acs.analchem.5b04409.
- Dong, Y., Li, B., Malitsky, S., Rogachev, I., Aharoni, A., Kaftan, F., Svatoš, A., Franceschi, P. Sample Preparation for Mass Spectrometry Imaging of Plant Tissues: A Review. *Front Plant Sci* **7**, 60 (2016) doi: 10.3389/fpls.2016.00060.
- Harris, A., Roseborough, A., Mor, R., Yeung, K. K.-C. & Whitehead, S. N. Ganglioside Detection from Formalin-Fixed Human Brain Tissue Utilizing MALDI Imaging Mass Spectrometry. *J. Am. Soc. Mass Spectrom.* **31**, 479-487 (2020) doi.org/10.1021/jasms.9b00110.
- Houdelet, C., Arafah, K., Bocquet, M., Bulet, P. Molecular histoproteomy by MALDI mass spectrometry imaging to uncover markers of the impact of *Nosema* on *Apis mellifera*. *Proteomics* **22**, 1-16 (2022) doi.org/10.1002/pmic.202100224.
- Qin, L., Zhang, Y., Liu, Y., He, H., Han, M., Li, Y., Zeng, M., Wang, X. Recent advances in matrix-assisted laser desorption/ionisation mass spectrometry imaging (MALDI-MSI) for *in situ* analysis of endogenous molecules in plants. *Phytochem. Anal.* **29**, 351-364 (2018) doi: 10.1002/pca.2759.
- Källback, P., Nilsson, A., Shariatgorji, M. & Andrén, P. E. msiQuant – Quantitation Software for Mass Spectrometry Imaging Enabling Fast Access, Visualization, and Analysis of Large Data Sets. *Anal. Chem.* **88**, 4346–4353 (2016) doi: 10.1021/acs.analchem.5b04603.
- Nunes, T. M. *et al.* Queen signals in a stingless bee: suppression of worker ovary activation and spatial distribution of active compounds. *Sci. Rep.* **4**, 7449 (2015) doi: 10.1038/srep07449.
- Porta, T., Lesur, A., Varesio, E. & Hopfgartner, G. Quantification in MALDI-MS imaging: what can we learn from MALDI-selected reaction monitoring and what can we expect for imaging? *Anal. Bioanal. Chem.* **407**, 2177-2187 (2015) doi: 10.1007/s00216-014-8315-5.
- Pratavieira, M., da Silva Menegasso, R.A., Caviquioli Garcia A.M., Simões Dos Santos, D., Gomes P.C., Malaspina, O., Palma M.S. MALDI Imaging Analysis of Neuropeptides in the Africanized Honeybee (*Apis mellifera*) Brain: Effect of Ontogeny. *J. Proteome Res.* **13**, 3054-3064 (2014) doi: 10.1021/pr500224b.
- Pratavieira, M., da Silva Menegasso, A.R., Grego Esteves, F., Sato, K.U., Malaspina, O., Palma, M.S. MALDI Imaging Analysis of Neuropeptides in Africanized Honeybee (*Apis mellifera*) Brain: Effect of Aggressiveness. *J. Proteome Res.* **17**, 2358-2369 (2018) doi: 10.1021/acs.jproteome.8b00098.
- Pratavieira, M., da Silva Menegasso, A.R., Roat, T., Malaspina, O. & Palma, M.S. *In Situ* Metabolomics of the Honeybee Brain: The Metabolism of L-Arginine through the Polyamine Pathway in the Proboscis Extension Response (PER). *J. Proteome Res.* **19**, 832-844 (2020) doi: 10.1021/acs.jproteome.9b00653.
- Rzagalinski, I. & Volmer, D. A. Quantification of low molecular weight compounds by MALDI imaging mass spectrometry - A tutorial review. *Biochim. Biophys. Acta Proteins Proteomics* **1865**, 726-739 (2017) doi: 10.1016/j.bbapap.2016.12.011.

Schulz, S., Becker, M., Groseclose, M. R., Schadt, S. & Hopf, C. Advanced MALDI mass spectrometry imaging in pharmaceutical research and drug development. *Curr. Opin. Biotechnol.* **55**, 51-59 (2019) doi: 10.1016/j.copbio.2018.08.003.

Seeley, E. H. & Caprioli, R. M. MALDI imaging mass spectrometry of human tissue: method challenges and clinical perspectives. *Trends Biotechnol.* **29**, 136-143 (2011) doi.org/10.1016/j.tibtech.2010.12.002.

Swales, J. G., Hamm, G., Clench, M. R. & Goodwin, R. J. A. Mass spectrometry imaging and its application in pharmaceutical research and development: A concise review. *Int. J. Mass Spectrom.* (2018) doi:10.1016/j.ijms.2018.02.007.

Verhaert, P. D., Conaway, M. C. P., Pekar, T. M. & Miller, K. Neuropeptide imaging on an LTQ with vMALDI source: The complete 'all-in-one' peptidome analysis. *Int. J. Mass Spectrom.* **260**, 177-184 (2007) doi.org/10.1016/j.ijms.2006.11.008.

Zhang, Y., Chen, D., Xu, Y., Ma, L., Du, M., Li, P., Yin, Z., Xu, H., Wu, X. Stereoselective toxicity mechanism of neonicotinoid dinotefuran in honeybees: New perspective from a spatial metabolomics study. *Sci. Total Environ.* (2022); 809:151116 doi: 10.1016/j.scitotenv.2021.151116.

Zhou, Q., Fülöp, A. & Hopf, C. Recent developments of novel matrices and on-tissue chemical derivatization reagents for MALDI-MSI. *Anal. Bioanal. Chem.* (2020) doi:10.1007/s00216-020-03023-7.